RI 9206

RI | 9206

REPORT OF INVESTIGATIONS/1988

Model of Coal Dust Explosion Suppression by Rock Dust Entrainment

By John C. Edwards and Kathleen M. Ford

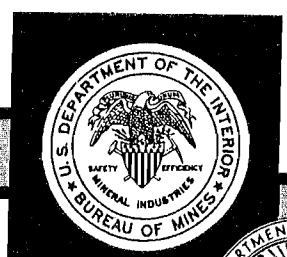

BUREAU OF MINES

UNITED STATES DEPARTMENT OF THE INTERIOR

Report of Investigations 9206

Model of Coal Dust Explosion Suppression by Rock Dust Entrainment

By John C. Edwards and Kathleen M. Ford

UNITED STATES DEPARTMENT OF THE INTERIOR
Donald Paul Hodel, Secretary

BUREAU OF MINES
T S Ary, Director

Library of Congress Cataloging in Publication Data:

Edwards, John C.
Model of coal dust explosion suppression by rock dust entrainment.

(Report of investigations; 9206)

Bibliography: p. 13.

Supt. of Docs. no.: I 28.23:9206.

1. Mine explosions—Mathematical models. 2. Coal mines and mining—Safety measures—Mathematical models. 3. Coal mines and mining—Dust control—Mathematical models. I. Ford, Kathleen M. II. Title. III. Series: Report of investigations (United States. Bureau of Mines); 9206.

TN23.U43 [TN313] 622 s [622'.8] 88-600215

CONTENTS

ILLUSTRATIONS

TABLES

UNIT OF MEASURE ABBREVIATIONS USED IN THIS REPORT

°C	degree Celsius
$cal \cdot cm^{-1} \cdot s^{-1} \cdot K^{-1}$	calorie per centimeter per second per degree kelvin
$cal \cdot g^{-1} \cdot K^{-1}$	calorie per gram per degree kelvin
cm	centimeter
cm^2	square centimeter
cm^3	cubic centimeter
$cm \cdot s^{-1}$	centimeter per second
$cm^2 \cdot s^{-1}$	square centimeter per second
$dyne \cdot cm^{-2}$	dyne per square centimeter
$erg \cdot K^{-1} \cdot mol^{-1}$	erg per degree kelvin per mole
ft	foot
g	gram
$g \cdot cm^{-3}$	gram per cubic centimeter
$g \cdot cm^{-4}$	gram per square centimeter per square centimeter
$g \cdot cm^{-1} \cdot s^{-1}$	gram per centimeter per second
$g \cdot cm^{-2} \cdot s^{-1}$	gram per square centimeter per second
$g \cdot cm^{-3} \cdot s^{-1}$	gram per cubic centimeter per second
K	kelvin
m	meter
m^2	square meter
mm	millimeter
μm	micrometer
ms	millisecond
$m \cdot s^{-1}$	meter per second
pct	percent
s	second

MODEL OF COAL DUST EXPLOSION SUPPRESSION BY ROCK DUST ENTRAINMENT

By John C. Edwards[1] and Kathleen M. Ford[2]

ABSTRACT

The Bureau of Mines developed a mathematical model to calculate the aerodynamically induced lifting of coal and rock dust from a composite deposition on a mine entry floor and the subsequent transport of the dust ahead of the propagating combustion zone of a coal dust explosion. For a series of experimental explosibility tests approximated by combustion zones that expand at a constant flame velocity, the mass fraction of airborne rock dust ahead of the flame front, as well as the mass fraction overtaken by the combustion zone, was calculated. A statistical analysis of the theoretical results demonstrated with a high level of confidence that the propagating and nonpropagating test samples belonged to separate populations. This analysis was further supported by an independent model of the average temperature over the combustion zone.

[1]Research physicist.
[2]Physical science technician.
Pittsburgh Research Center, Bureau of Mines, Pittsburgh, PA.

INTRODUCTION

Coal dust was identified as an active cause in mine explosions as early as 1844 by Faraday (*1*),[3] although his viewpoint was not widely accepted for another 50 years. There has been a worldwide effort to understand the significant factors involved in coal dust explosions and their prevention and suppression. A historical summary of research into the causes of coal dust explosions and methods of suppression is given by Cybulski (*1*). Since 1910, the Bureau of Mines has carried out research on methane and coal dust explosions in its experimental mine (*2-5*). Effects of methane gas and coal dust concentrations, dust particle sizes, and inerting agents in single-entry explosions have been the subject of this research.

A coal dust explosion in a mine entry can be initiated by a methane-air explosion that generates sufficient air pressure to disperse coal dust from the entry surfaces into the expanding combustion zone. Heat transfer to the coal dust particles results in the production of volatiles and tars from these particles. The combustible devolatilization products react with the oxygen in the air at elevated temperatures. Heat released from this exothermic reaction is converted into mechanical work of expansion of the semiconfined air. This fluidizes and disperses additional coal dust from the entry surfaces into the propagating coal dust explosion. The propagation of the combustion zone is limited by the turbulent mixing of the hot products at the leading edge of the combustion zone, the flame front, with the coal dust-air mixture.

An important consideration in mine safety is the suppression of an incipient coal dust explosion. One safety measure is the dilution of the combustible coal dust with rock dust (calcium carbonate). In a coal mining operation, rock dust is applied to the entry roof, ribs, and floor. Should a coal dust explosion be initiated, the rock dust would be entrained along with the coal dust into the airstream. The dispersed rock dust acts as a thermal sink, with the transfer of thermal energy by conduction and convection, and as a means of blocking radiant energy transfer to the coal particles, thereby inhibiting the propagation of the coal dust explosion.

A qualitative description of a coal dust explosion and the principal mechanisms can be inferred from measured quantities. The objective of this report is to develop, through a mathematical model, a quantitative description of the entrainment of inerting materials, specifically rock dust, by a propagating coal dust explosion. Model predictions of dust concentrations overtaken by the explosion are correlated with full-scale explosion test data involving propagating and nonpropagating dust explosions. A similar correlation is made between the calculated average temperature over the combustion zone and explosion behavior.

The most recent studies of the effectiveness of rock dust in the suppression of methane-initiated coal dust explosions were reported by Sapko, Weiss, and Watson of the Bureau (*5*). These tests were designed to gauge how much, and in what manner of distribution on the entry floor, rock dust should suppress float coal dust explosions, and they provided comparison data for the model presented in this report. The model was used to evaluate the ratio of the mass of rock dust to the mass of rock plus coal dust at the leading edge of the flame zone and that ratio in the region overtaken by the propagating combustion zone. Correlations were made between the experimental results, which characterized explosions as propagating or nonpropagating, and the mass fraction of rock dust at the flame front and overtaken by the combustion zone.

Additional comparisons were made in terms of the measured gas pressure within and ahead of the combustion zone. From the measured pressure distribution, an average gas temperature over the combustion zone could be calculated as demonstrated by Lunn and Roberts (*6*). These average temperatures were less than the combustion temperature of coal dust, a phenomenon reported (*6*) for coal dust explosion tests performed at the Health and Safety Executive, Buxton, United Kingdom. Lunn and Roberts observed that this is indicative of incomplete combustion behind the flame front, with, most probably, regions of localized combustion adjacent to combustion-free regions.

DUST TRANSPORT MODEL

FLAME DESCRIPTION

Predicting the lifting of dust from an entry surface and its subsequent transport requires a description of the aerodynamics that precedes the flame front generated by the combustion zone. A complete description of the combustion zone reaction must be generated from detailed kinetic equations and the Navier-Stokes equations, and coupled to the hydrodynamic motion ahead of the flame. However, in this report, an empirical representation of the propagating flame is obtained and the aerodynamics is determined in a treatment that replaces the flame front with a nonuniformly accelerated surface, or piston.

The former computational approach to the study of explosions has been utilized by Green, Piper, and Upfold (*7*) and Phillips (*8*) in a two-fluid model and by Vassart (*9*) in a model that uses the time average of the dependent

[3]Italic numbers in parentheses refer to items in the list of references preceding the appendixes.

variables. These approaches are numerically complex but quite useful for a fundamental investigation of the initiation and development of an explosion. For this study, the primary emphasis is upon the dust lifting and entrainment for known rates of combustion zone expansion, and therefore, the inherent simplicity and utility of an approximate model that represents the flame front as a moving surface is suitable.

The representation of the flame by an analytical expression was utilized by Wingfield (*10*) in the analysis of methane explosions. In this analysis, the flame motion is represented as a nonuniformly accelerated piston. The flame front position is related to the elapsed time by

$$x_f = \frac{a}{b} t^b, \tag{1}$$

where x_f = flame position, m,

a = parameter in kinematic expression for flame position, $m \cdot s^{-1}$,

b = exponent of time in kinematic expression for flame position,

and t = time, s.

Jones (*11*) developed the aerodynamics ahead of the flame front for a uniformly accelerated motion, i.e., b = 2. Although this is also treated by Landau and Lifshitz (*12*, pp. 370-372), the uniqueness of Jones' treatment resides in the postulation that the gas velocity at the flame is related to the flame velocity through a time-dependent proportionality $\beta(t)$:

$$u_f = \beta v_f, \tag{2}$$

$$v_f = a t^{b-1}, \tag{3}$$

where u_f = gas velocity at flame front, $m \cdot s^{-1}$,

v_f = flame velocity, $m \cdot s^{-1}$,

and β = ratio of gas to flame velocity.

Jones results have been generalized in this report to b $\neq$ 2.

The value of β is always less than 1 and, in the analysis of Jones (*11*), is restricted to be a constant. In particular, a typical value of 0.9 was suggested in reference 11. Pickles (*13*) established a proportionality between v_f and u_f based upon an estimation of the longitudinal diffusion coefficient for turbulent flow:

$$v_f - u_f \sim \frac{1}{3} u_f. \tag{4}$$

For a nearly constant β, equations 2 and 4 identify β = 0.75. Equation 4 is an empirical correlation for the burning velocity. Its development assumes the flow is confined to a cylindrical duct.

The physics implied by β < 1 is that the flame is represented by a semipermeable piston. This is a reasonable interpretation of a flame as a surface of discontinuity that overtakes a fuel-air mixture. The aerodynamic in front of the moving piston is well understood (*11-13*). If b > 2, a traveling wave is formed in the gas adjacent to the piston, and eventually a shock develops at a location intermediate between the piston and the sonic wave front. A value b = 2 results in the formation of a shock at the sonic wave front a finite time after the piston motion commences. If b < 2, a shock is formed at the piston front when its motion is initiated.

For the case $b \geq 2$, it can be shown (*12*) that the gas velocity u(x,t) in the traveling wave generated by the piston is uniquely determined at spatial location x and time t prior to the shock formation from

$$x = \left[u + c_o + \frac{1}{2}(\gamma - 1)u\right] t + \frac{a}{b}\left(\frac{u}{\beta a}\right)^{\frac{b}{b-1}} - \left[\frac{1}{2}(\gamma + 1)\, u + c_o\right]\left(\frac{u}{\beta a}\right)^{\frac{1}{b-1}}, \tag{5}$$

where x = position coordinate, m,

u = gas velocity, $m \cdot s^{-1}$,

c_o = isentropic speed of sound in undisturbed gas ahead of wave, $m \cdot s^{-1}$,

and γ = adiabatic exponent.

For b > 2, a shock is formed at time, t_s,

$$t_s = \left(\frac{2c_o}{a}\right)^{\frac{1}{b-1}} \frac{1}{\gamma + 1} \frac{1}{\beta}\left[\frac{\beta(\gamma + 1)b - 2}{b - 2}\right]^{\frac{b-2}{b-1}}, \tag{6}$$

whereas for b = 2, a shock is formed at

$$t_s = \frac{2c_o}{(\gamma + 1)a\beta}. \tag{7}$$

The case b < 2 results in the formation of a shock at the piston surface simultaneously with the commencement of the piston motion. The special case b = 1 is amenable to an analytic solution for the gas velocity and shock position in the manner described in reference 12 (pp. 357-358). The gas velocity ahead of the piston is equal to the gas velocity at the piston surface, and the shock position x_s is dependent upon the flame velocity:

$$x_s = \left[\frac{1}{4} (\gamma + 1)\, u_f + \sqrt{\frac{1}{16} (\gamma + 1)^2\, u_f^2 + c_o^2} \right] t. \quad (8)$$

The results can be used to determine the gas velocity ahead of a flame described by the parametric equation 1, for b = 1 and b ≥ 2. The gas velocity ahead of the flame front will be used to determine the erosion and transport of dust initially in situ on the mine entry floor.

DUST TRANSPORT EQUATION AND NUMERICAL METHOD

The dust particles on the entry floor that are fluidized by the aerodynamic disturbance ahead of the flame front and entrained into the airflow are treated as a high-molecular-weight gas. The boundary layer development on the mine floor and the vertical transport of the dust particles into the gas are not evaluated. Instead, it is assumed that the dust particles are instantaneously and uniformly distributed over the cross section of the mine entry. Aerodynamic slip of the particles is neglected, as well as the gravitational settling of the particles. The particles, upon being lifted from the entry floor, are transported by a unidirectional gas flow field, u(x,t), established ahead of the advancing flame (piston). The conservation-of-species equation for coal (k = 1), rock dust (k = 2), air (k = 3), and total gas (k = 4), with the assumption the coal and rock dust are high-molecular-weight gases, is a nonlinear dust transport equation for the mass density of species k:

$$\frac{\partial}{\partial t} \rho_k + \frac{\partial}{\partial x} (u \rho_k) = \rho_4 D \frac{\partial^2}{\partial x^2} \left[\frac{\rho_k}{\rho_4} \right] + \dot{r}_k, \quad (9)$$

for k = 1,4,

where $\rho_4 = \sum_{k=1}^{3} \rho_k$,

ρ_k = mass density for species k, $g \cdot cm^{-3}$,

$\dot{r}_k$ = addition rate of species k, $g \cdot cm^{-3} \cdot s^{-1}$,

and D = diffusion coefficient, $cm^2 \cdot s^{-1}$.

Equation 9 applies throughout the mine entry.

The first term on the right side of equation 9 describes the dispersion of the particles, and the second term, a production term, describes the addition of coal and rock dust to the airstream. The numerical method used to solve equation 9 is discussed in appendix A.

Turbulent dispersion in the model is proportional to the gradient of the particle concentration in the airstream along the longitudinal direction. Instantaneous mixing in the transverse direction is assumed. The intensity of the dispersion, D/ud, is related in graphical form to the Reynolds number, $R_e = du\rho/u$, in Levenspiel (*14*). The characteristic length d is identified with the equivalent diameter for rectangular roadways, which is four times the hydraulic radius. Evaluation of the Reynolds number is made for a gas density (∂) of 1.3×10^{-3} $g \cdot cm^{-3}$ and a dynamic viscosity (μ) of 1.8×10^{-4} $g \cdot cm^{-1} \cdot s^{-1}$. The length d for 6- by 9-ft cross section of the experimental gallery is 220 cm. A gas flow of 50 $m \cdot s^{-1}$ for the specified mine entry defines a Reynolds number equal to 8×10^6. The results in reference 14 show that for $R_e > 10^5$, the quantity D/ud is approximately 0.2.

Some discussion is in order about the relationship of production term $\dot{r}_k$ to the mass injection rate $\dot{m}''$ of coal and rock dust from the entry surface. For a uniform dispersion over the cross section of the entry, the production term is the ratio of mass injected from the floor surface area to the volume of the entry extending the length of the floor surface under consideration:

$$\dot{r}_k = \int_S \dot{m}'' ds \Big/ \int_V dv, \quad (10)$$

where S = entry floor surface area, cm^2,

V = entry volume, cm^3,

$\dot{m}''$ = mass injection rate, $g \cdot cm^{-2} \cdot s^{-1}$,

ds = differential surface area, cm^2,

and dv = differential volume, cm^3.

For a uniform rectangular entry cross section of height h,

$$\dot{r}_k = \dot{m}''/h, \text{ for } k = 1,2. \quad (11)$$

The specific form of $\dot{m}''$ is discussed in the next section.

Prior to the arrival of the sonic disturbance generated by the flame front at the exit to the mine roadway, the constraint $\dot{r}_3 = 0$ is valid, and

$$\dot{r}_4 = (\dot{r}_1 + \dot{r}_2). \quad (12)$$

DUST-LIFTING MODEL

The dust source term $\dot{m}''$ is based upon complex aerodynamic interactions between the gas flow ahead of the flame front and the dust particles at rest upon the entry floor. Bagnold (*15*), Chepil (*16*), and Zingg (*17*) have proposed expressions for the mass flux of sand and soil from a surface. Their models relate the mass flux to the cube of the gas friction velocity at the surface, which is an indicator of the turbulence level; these models are applicable to particles transported by saltation, the process whereby particles are injected vertically into the airstream and descend with a flat trajectory to impinge upon the surface, whereupon another particle is dislodged. If saltation does not occur, surface creep, whereby particles move along the

floor, could still occur. Travis (*18*) characterized transport models of saltation and surface creep in terms of the particle diameter. Saltation occurs for particles with diameters between 50 and 1,000 μm. When the aerodynamic forces are inadequate to lift the particles and the particle diameter is greater than 1,000 μm, surface creep can occur.

For flow between flat plates, representative of the mine entry roof and floor, the frictional velocity and the horizontal wind speed are linearly proportional. The cubic dependence of the mass flux upon wind speed for the saltation models is in accord with Dawes' (*19-21*) result that the rate of dust lifting by erosion is proportional to the cube of the gas velocity.

A recent model of the scouring of dust from a surface was proposed by Rosenblatt.[4] The mass flux is uniquely determined by the local gas density and velocity:

$$\dot{m}'' = \left(0.0021\, u^{0.25} - \frac{4}{u} \right) \rho u. \qquad (13)$$

The ratio of the mass flux to the gas momentum flux depends solely upon the gas velocity. Equation 13 implies a threshold gas velocity of 420 cm $\cdot$ s^{-1} for dust lifting to occur. This value corresponds well to the experimentally determined threshold velocities of 5 and 8 m $\cdot$ s^{-1} for the lifting of coal and rock dust as reported by Dawes (*19-21*).

Dust lifting will be affected by the free moisture and the associated cohesion of the dust. If the cohesion is significant, Dawes (*19*) reported that an entire layer of dust, or a portion of the layer, will be lifted (denudation). For a lower cohesion, erosion, the particle-by-particle removal of dust, will occur. These phenomena depend also upon the bulk density of the particles. Dawes (*19*) established that if the ratio of the square of the bulk density to the cohesion (tensile breaking strength) is less than 6 g $\cdot$ cm^{-4}, denudation occurs, and if the ratio is greater than 6, erosion occurs. Singer, Harris, and Grumer (*22*) examined the dispersal of coal and rock dusts by blasts of air generated by gas explosions and found the threshold velocities to be in the range of 5 to 30 m $\cdot$ s^{-1}. In the applications reported here, equation 13 is used to describe the dust lifting. The distinction between erosion and denudation is ignored.

The utilization of the dust-lifting source term ($\dot{m}_k$) in equation 9 requires a proper accounting for the dust removed from the source. The mass flux ($\dot{m}''$) is independent of the type of dust and the particle size. For a uniform mixture of rock and coal dust, the source term is weighted by the appropriate mass fraction. As shown in figure 1, there are two dust-layer regions. The first layer of length ℓ_o consists of coal dust in a layer of thickness h_o. This layer is adjacent to a layer of length ℓ_1 consisting of a float coal dust layer of thickness $h_2 - h_1$ that rests upon a substratum of thickness h_1. The substratum is a homogeneous mixture of coal and rock dust. The bulk density of the substratum is defined in terms of the substratum porosity, rock and coal dust particle densities, and rock dust mass fraction:

$$\rho_B = (1 - \phi) \Big/ \left(\frac{f}{\rho_R} + \frac{1 - f}{\rho_C} \right), \qquad (14)$$

where ρ_B = bulk density, g $\cdot$ cm^{-3},

ϕ = porosity,

f = rock dust mass fraction in substratum,

[4]Private communication from M. Rosenblatt, California Research & Technology, Inc., Chatsworth, CA, 1987.

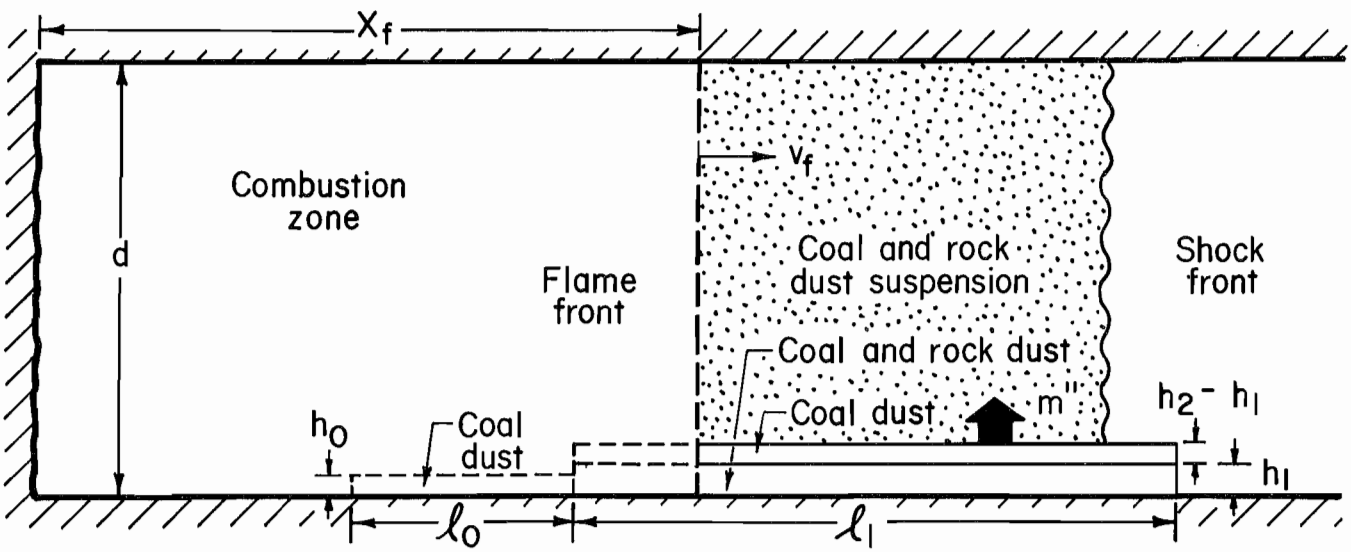

Figure 1.—Schematic of coal-rock dust layers on entry floor. See appendix B for identification of symbols.

ρ_R = rock dust particle density, $g \cdot cm^{-3}$,

and ρ_C = coal dust particle density, $g \cdot cm^{-3}$.

The physical properties used in this report for rock and coal dust are listed in table 1. The bulk density of the float coal dust layer and the coal dust in the booster zone, the region of length ℓ_0 containing only coal dust, is 0.75 $g \cdot cm^{-3}$. The bulk density is used in the computation to determine the thickness of the dust layer removed for a known mass flux.

TABLE 1. - Physical properties of rock and coal dust

ϕ		0.53
ρ_R	$g \cdot cm^{-3}$	2.753
ρ_C	$g \cdot cm^{-3}$	1.328
C_p	$cal \cdot g^{-1} \cdot K^{-1}$	0.24
λ_c	$cal \cdot cm^{-1} \cdot s^{-1} \cdot K^{-1}$	4.78×10^{-4}

CHARACTERIZATION OF EXPLOSION

It is intended to characterize explosions as propagating or nonpropagating based upon the proportion of rock dust in the rock-coal dust mixture overtaken by the spreading explosion. The explosion is considered to be propagating if the flame extends sufficiently far beyond the dusted test zone. The heat liberated by the combustion of the volatiles released by the coal particles results in an increase in the product gas temperature and a further expansion of the hot product gases into the unreacted coal dust dispersed ahead of the advancing flame. This process is moderated through the absorption of heat by the rock dust.

The mode of the flame propagation is characterized by an analysis of the time constants in the combustion process. The controlling time step in the absence of rock dust in a propagation can be determined through an evaluation of the time constants for (1) heating of the coal dust particle, τ_1, (2) devolatilization and product combustion, τ_2, and (3) turbulent mixing of the hot products with the unreacted coal dust and air mixture, τ_3.

The time constant for particle heating is related to the particle density, specific heat, thermal conductivity, and radius:

$$\tau_1 = \frac{1}{3} \frac{\rho_C C_p R^2}{\lambda_c}, \qquad (15)$$

where C_p = particle specific heat, $cal \cdot g^{-1} \cdot K^{-1}$,

R = particle radius, cm,

and λ_c = particle thermal conductivity, $cal \cdot cm^{-1} \cdot s^{-1} \cdot K^{-1}$.

Equation 15 assumes that heat transfer is by conduction from the hot combustion products. For a 74-μm-diameter coal dust particle–80 pct of the float coal dust used in Bureau tests (*5*) had a smaller diameter–and for the physical properties listed in table 1, the value of τ_1 is approximately 3 ms.

Estimates for the burning time for an isolated coal particle were reported by Hedley and Hedley (*23*). The values reported are for the complete combustion of the coal particle, both volatiles and the solid phase. It is likely that the volatile combustion is the more important for flame propagation. Based upon the work of Field (*24*), Pickles (*13*) estimated a devolatilization time of 8 ms and a volatile combustion time of 7 ms for a 50-μm coal particle at 1,000° C. For an estimate of τ_2, 15 ms is used.

Pickles estimated the time scale τ_3 for turbulent mixing from the entry diameter and friction velocity:

$$\tau_3 \sim 0.05 d/u^*, \qquad (16)$$

where d = entry diameter, m,

u^* = wall friction velocity, $m \cdot s^{-1}$.

The friction velocity is approximately one-thirtieth of the gas velocity. For flame velocities between 95 and 178 $m \cdot s^{-1}$, characteristic of the tests reported in reference 5, and an entry diameter of 2.2 m, the scale for turbulent mixing is approximately 19 to 34 ms. The ratio of τ_3 to $\tau_1 + \tau_2$ is between 1.1 and 1.9, which indicates that the limiting time step in the propagating combustion process is the turbulent mixing.

For a constant-velocity flame, the above analysis indicates that the time scales for coal particle combustion and turbulent mixing are comparable at a flame velocity of 183 $m \cdot s^{-1}$, 56 pct of the adiabatic sound speed. The availability of coal dust for turbulent mixing is controlled by the dust lifting, which is evaluated in this model.

The analysis of Pickles (*13*) concludes that if the time scale for turbulent mixing of the hot combustion products with the unburnt fuel is greater than the particle burning time, it is expected that burnt and unburnt fuel will reside in separate parcels within the combustion zone. If this is the case, it is reasonable to expect the average temperature over the combustion zone to be less than the combustion temperature of coal dust. This idea is developed in the "Results" section, which shows relativity low average temperatures predicted from measured gas pressures.

During the course of the turbulent flame spread, the computer program developed for the dust transport model evaluates the ratio of rock dust to total dust overtaken by the flame. This ratio is expected to show a significant difference between propagating and nonpropagating coal dust explosions when it is evaluated at a fixed location for the various test conditions. The total rock dust mass and coal dust mass overtaken by the combustion zone in an entry of cross-sectional area A are evaluated from the airborne mass densities at the flame front for a constant flame velocity:

$$M_C = (1 - \beta) v_f A \int_0^t \rho_1 (x_f, s)\, ds, \qquad (17)$$

$$M_R = (1 - \beta)\, v_f\, A \int_0^t \rho_2\,(x_f,s)\, ds, \qquad (18)$$

where M_C = coal dust mass overtaken by combustion zone, g,

M_R = rock dust mass overtaken by combustion zone, g,

A = cross-sectional area of mine entry, m^2,

and ds = differential time, s.

The ratio $M_R/(M_R + M_C)$, designated M_{RC}, can be examined as a characterization of the flame, which is propagating or nonpropagating. A nonpropagating flame would be expected to have a larger ratio, since the ratio is directly related to the energy available to sustain a propagating explosion.

Since the ratio of rock dust to total available dust is expected to be a characteristic that distinguishes a propagating from a nonpropagating explosion, it is expected that the average temperature in the combustion region of a nonpropagating dust explosion will be less than in a propagating explosion. The latter hypothesis can be evaluated through a comparison of predicted average temperatures. In a fundamental sense, the temperature in the combustion zone depends upon the reaction kinetics of the volatiles thermally driven off from the coal particles. A computation of the temperature in the combustion zone is a complex numerical problem. For the analysis in this report, an estimation of an average temperature over the combustion zone is made from the known pressure field in and ahead of the combustion zone.

CALCULATED AVERAGE TEMPERATURE OVER COMBUSTION ZONE

A coal dust explosion is driven by the difference between the energy released by the combustion of the coal dust and that lost to the rock dust. A measure of this net energy is the average temperature over the combustion zone, which can be evaluated from the measured gas pressure in the mine entry. A correlation should exist between the average temperature and the classification of the explosion as propagating or nonpropagating.

The heat released in the combustion zone of a semiconfined coal dust explosion is partly converted into a temperature rise of the gas mixture and partly converted into work of expansion of the gas. Lunn and Roberts (*6*) demonstrated in their study of hybrid methane-coal dust explosions how the average temperature over the combustion zone of length x_f depends upon the mass of gas and the gas pressure behind the combustion front prior to the arrival of the sonic disturbance generated by the flame front at the exit of the mine roadway. From the ideal gas law for an average temperature over the combustion zone of length x_f, it was shown (*6*) that

$$\bar{T}_B(t) = \frac{W}{R_g} A \int_0^{x_f} P(x,t)\, dx / m_B(t), \qquad (19)$$

where $\bar{T}_B$ = average temperature in combustion zone, K,

W = gas molecular weight,

R_g = gas constant, 8.3143×10^7 erg · K^{-1} · mol^{-1},

A = cross-sectional area of mine entry, cm^2,

P = gas pressure, dyne · cm^{-2},

dx = differential distance, cm,

and m_B = mass of gas in combustion zone, g.

The quantity $m_B(t)$ is evaluated as the difference between the initial mass of gas (m_o) in the entry and the mass of gas $m_A(t)$ ahead of the flame front. For an adiabatic compression of the gas ahead of the flame, $m_A(t)$ is evaluated from the gas density $\rho(x,t)$ ahead of the flame:

$$m_A(t) = A \int_{x_f}^{\ell} \rho(x,t)\, dx \qquad (20)$$

$$= A \frac{W}{R_g T_o} P_o^{1 - \frac{1}{\gamma}} \int_{x_f}^{\ell} P^{\frac{1}{\gamma}}(x,t)\, dx, \qquad (21)$$

where m_A = mass of gas ahead of flame front, g,

T_o = gas ambient temperature, K,

P_o = gas ambient pressure, dyne · cm^{-2},

γ = adiabatic exponent,

and ℓ = entry length, cm.

Equations 19 through 21 are used to evaluate the average gas temperature over the combustion zone from the experimentally measured gas pressures. The integrals of the powers of the pressure are evaluated numerically with either the trapezoidal rule or Simpson's extended integration rule. The choice of method depends upon whether an even or odd number of values of the dependent variable, the pressure, are available over the integration interval. As pointed out by Lunn and Roberts (*6*), the calculated average temperature in the combustion zone may be significantly less than the combustion temperature of coal

products. This is possible in the event of incomplete mixing of the hot combustion products with the coal dust as the flame propagates.

It is expected that a correlation should exist between the average temperature over the combustion zone and whether the coal dust explosion is characterized as propagating or nonpropagating. This average temperature should be a consequence of the ratio of rock to coal dust. As a result of incomplete mixing of the products with the reactants, the measured value of the local temperature will be quite different from the average temperature throughout the gas zone, and a direct linkage between the average combustion zone temperature and the mass of coal dust and rock dust entrained into the combustion zone is not obvious.

In the "Results" section, the model is applied to the prediction of the coal and rock dust entrained by the expanding combustion zone and to the prediction of the average combustion zone temperature, for the dust explosion conditions reported in reference 5.

RESULTS

The dust lifting and transport model was developed into a Fortran computer program that could be applied to a prescribed test configuration in which the dust loading and flame displacement were specified. The explosibility tests reported by Sapko, Weiss, and Watson (5) were analyzed. For each test, a carefully prescribed mixture of coal and rock dust was distributed over a specified entry floor length. As shown in figure 1, a pure coal dust layer was adjacent to a composite layer that consisted of a float coal dust layer resting upon a substratum of coal and rock dust. The coal dust layer of length ℓ_0 = 15 m was distributed over the distance 15 to 30 m from the entry face. The composite layer of coal and rock dust of length ℓ_1 = 91 m adjoined the pure coal dust layer. The coal dust explosions were initiated with a methane-air explosion at the entry face for a variety of test conditions corresponding to variations in the thickness $h_2 - h_1$ of the float coal dust layer and mass fraction of rock dust in the substratum. In each test, the thickness h_0 of the 15-m coal dust layer was 0.072 cm, and the thickness h_1 of the substratum was 0.8 cm.

The flame position was recorded as a function of time, and the data were fitted to equation 1 with b = 1 for tests reported in reference 5. In this application, the detailed acceleration and deceleration of the flame is neglected. As discussed in the section "Flame Description," the gas flow is constant for the case b = 1, and the shock front is described by equation 8. This analytic result is used in the model calculations. Table 2 enumerates for each test the float dust thickness and substratum rock dust concentration.[5] The test conditions for the majority of tests resulted in a natural pairing of tests with the same fixed-thickness float coal dust layer on top of the coal-rock dust substratum and two different rock dust concentrations in the substratum. The exceptions were tests 1, 6, and 11. The counterpart to test 11 was not available, and the counterparts to tests 1 and 6 were considered to have only marginal propagation. In each pair of tests, the greater rock dust concentration in the substratum corresponds to a nonpropagating explosion and the lower rock dust concentration to a propagating case.

TABLE 2. - Explosion test data

Test	Float coal dust layer thickness, mm	Substratum rock dust concentration, pct	Flame travel, ft	Explosion propagation[1]
1 . .	0.06	80	310	N
2 . .	.12	85	340	N
3 . .	.12	80	900	P
4 . .	.18	85	300	N
5 . .	.18	77.5	>900	P
6 . .	.24	82.5	750	P
7 . .	.36	87.5	280	N
8 . .	.36	85	740	P
9 . .	.48	90	350	N
10 .	.48	85	850	P
11 .	.66	80	>790	P

[1]P = propagating; N = nonpropagating.

Table 2 shows that the flame did not travel significantly beyond 300 ft for a nonpropagating explosion. For this reason, the analysis made with the transport model, equations 9, 12, and 13, was focused upon the airborne rock dust mass fraction (f_{RC}) at the 300-ft station when overtaken by the flame and upon the rock dust mass fraction (M_{RC}) residing throughout the combustion zone behind the flame front when the flame reached the 300-ft station. A variable parameter in the calculations is the parameter β in equation 2 (the ratio of gas to flame velocity). Results of the computations made with the dust transport model are shown in table 3 for β = 0.75 and in table 4 for β = 0.9. In accord with equation 3, the parameter a in table 3 is representative of the flame velocity. In each pair of tests corresponding to a fixed coal dust layer thickness and two base-layer rock dust concentrations, the airborne rock dust mass fraction (f_{RC}) was greater for a nonpropagating explosion than for a propagating explosion, when evaluated at the 300-ft station at the time of flame arrival. Similarly, the mass fraction M_{RC} of rock dust overtaken by

[5]Test numbers used in this report and the equivalent test identifications from reference 5 are as follows: 1–4055, 2–4054, 3–4043, 4–4056, 5–4042, 6–4068, 7–4057, 8–4069, 9–4051, 10–4064, 11–4053.

the flame at the 300-ft station was greater for a nonpropagating explosion than for a propagating explosion. However, among the tests considered, the rock dust mass fraction was not uniformly greater for nonpropagating cases than for propagating cases.

TABLE 3. - Calculated rock dust mass fractions f_{RC} and M_{RC} for β = 0.75

Test	Flame velocity [a(b = 1)], m · s^{-1}	f_{RC}	M_{RC}	Explosion propagation[1]
1	112	0.77	0.63	N
2	115	.80	.66	N
3	178	.75	.63	P
4	130	.77	.64	N
5	94.5	.71	.58	P
6	172	.74	.61	P
7	154	.73	.59	N
8	154	.71	.58	P
9	125	.69	.53	N
10	148	.66	.52	P
11	140	.56	.40	P

[1]P = propagating; N = nonpropagating.

TABLE 4. - Calculated rock dust mass fractions f_{RC} and M_{RC} for β = 0.9

Test	f_{RC}	M_{RC}	Explosion propagation[1]
1	0.74	0.62	N
2	.78	.66	N
3	.74	.64	P
4	.77	.66	N
5	.70	.59	P
6	.75	.64	P
7	.77	.66	N
8	.75	.64	P
9	.76	.65	N
10	.73	.62	P
11	.65	.55	P

[1]P = propagating; N = nonpropagating.

An overview of the situation is shown in figures 2 and 3. Figure 2 shows the relationship between the percentage of total incombustibles in the substratum, the float coal dust concentration equivalent to the float coal dust layer on the entry floor dispersed over the entry volume, and at the arrival of the flame at the 300-ft station, the predicted mass fraction of airborne rock dust (f_{RC}) for propagating and nonpropagating tests for β = 0.75. The results in figure 3 are for β = 0.9.

It is instructive to examine the time evolution of the predicted mass fraction values M_{RC} of rock dust overtaken by flame until the flame reaches the 300-ft station, for a pair of tests, one propagating and the other nonpropagating, in order to focus on the bias of the results toward the rock dust concentration in the substratum. The cases selected are tests 2 and 3, and the value of β is 0.9. The model-predicted mass fractions of rock dust overtaken by flame for both tests are shown in figure 4. The curves are similar, with a slightly greater value of M_{RC} for the nonpropagating case. The two tests, as shown in table 2, correspond to a fixed float coal dust layer thickness of 0.12 mm and substratum rock dust concentrations of 85 pct for test 2 and 80 pct for test 3. The flame arrival times for the two tests are 0.80 and 0.52 s, respectively.

Based upon the predicted values of f_{RC} and M_{RC} for the five propagating cases and the six nonpropagating cases in tables 3 and 4, an evaluation was made of the level of confidence that can be established with regard to the two samples' being members of two distinct populations of tests: one for propagating explosions and one for nonpropagating explosions. If the research hypothesis is that the population means are representative of distinct cases, with the population means of f_{RC} and M_{RC} always greater for nonpropagating explosions, then the null hypothesis to be disproved is that the samples are the same, i.e., the population means are identical. The test procedure for comparing two population means, developed in reference 25, uses Student's t-test. The null hypothesis is rejected, with a probability α of incorrect rejection, if the t-statistic satisfies

$$t = (\bar{y}_n - \bar{y}_p)/S_d \sqrt{1/n_n + 1/n_p} > t_\alpha, \qquad (22)$$

where

$\bar{y}_n$ and $\bar{y}_p$ = sample averages for nonpropagating and propagating tests, respectively,

n_n and n_p = number of data values in each sample,

S_d = estimate of common population standard deviation,

and t_α = value of t-statistic for probability α.

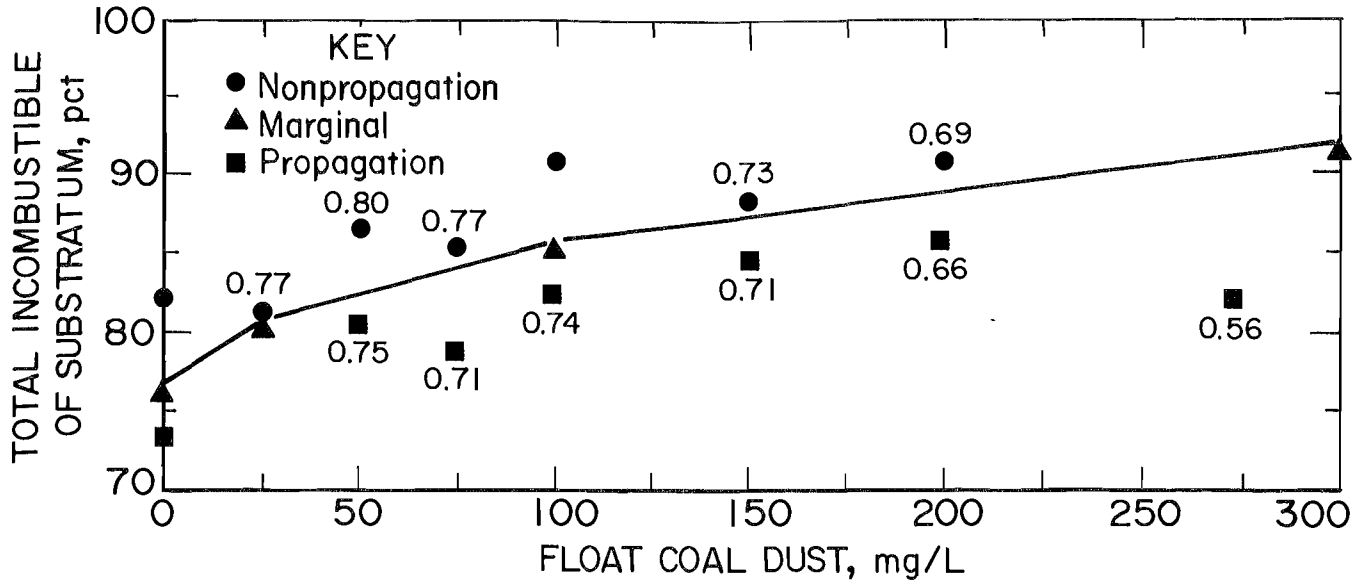

Figure 2.—Mass fractions of airborne rock dust at 300-ft station for various percentages of total incombustibles in substratum and various loadings of float coal dust, for β = 0.75. (There were insufficient test data for calculation of mass fractions of airborne rock dust for some tests.)

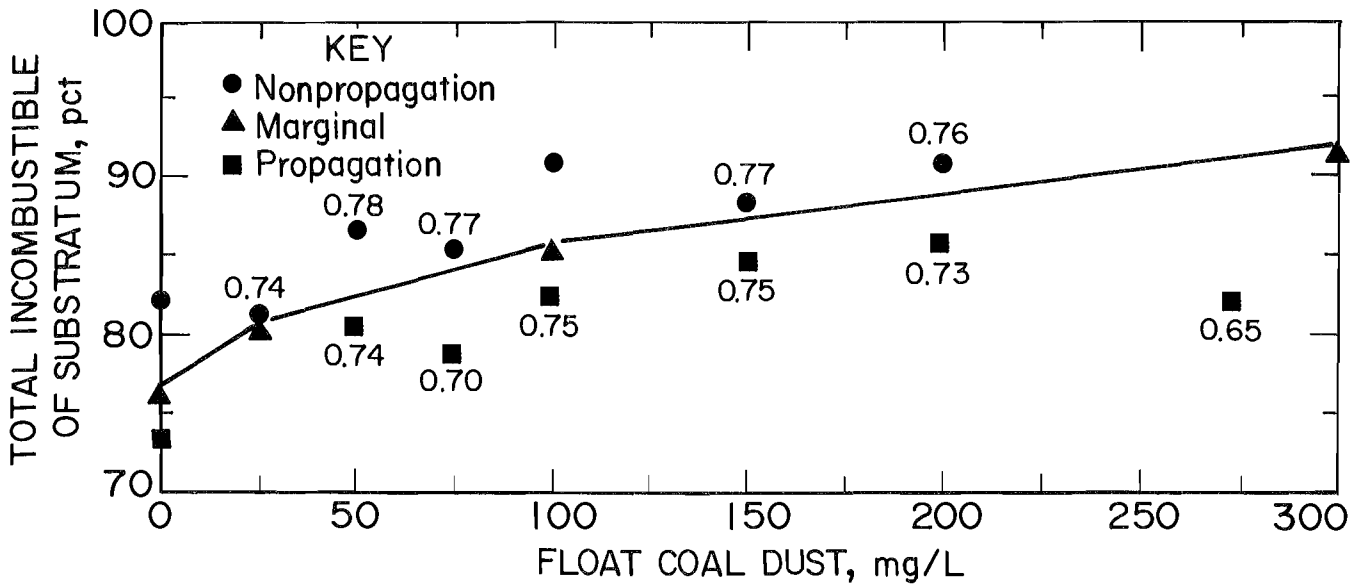

Figure 3.—Mass fractions of airborne rock dust at 300-ft station for various percentages of total incombustibles in substratum and various loadings of float coal dust, for β = 0.9. (There were insufficient test data for calculation of mass fractions of airborne rock dust for some tests.)

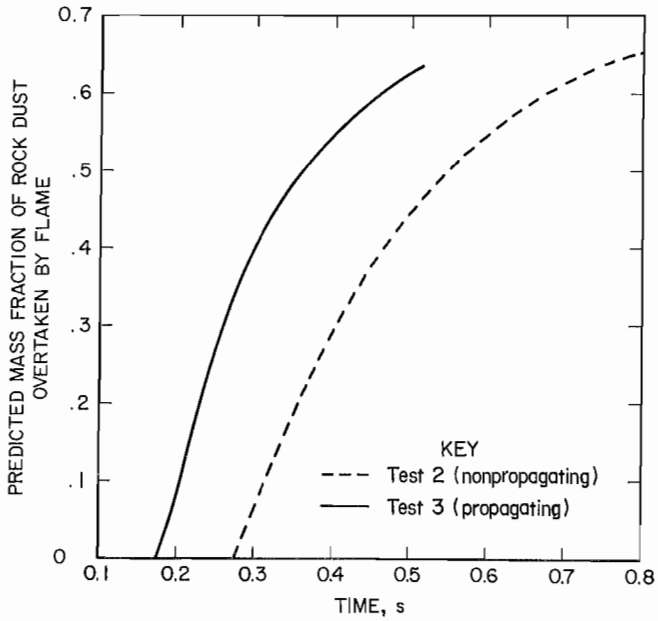

Figure 4.—Variation with time of mass fraction of rock dust overtaken by flame until flame's arrival at 300-ft station, tests 2 and 3.

The quantity S_d is based upon the sample variances S_n^2 and S_p^2:

$$S_d = \sqrt{\frac{(n_n - 1)\, S_n^2 + (n_p - 1)\, S_p^2}{n_n + n_p - 2}}. \qquad (23)$$

For the case $\beta = 0.75$ (table 3), sample means of 0.75 and 0.69 are calculated for the values of f_{RC} for the nonpropagating and propagating cases, respectively. The data within each sample are within ±2 sample standard deviations of the sample mean. The estimated common population standard deviation has a value of 0.062, and the t-statistic has a value of 1.70. In accord with the general assumption for application of Student's test, the smaller size sample has a smaller variance than the larger size sample. The null hypothesis that there is no difference in the mean value of f_{RC} between nonpropagating and propagating cases can be rejected for 9 degrees of freedom with a confidence of 6 pct for an incorrect rejection. This is equivalent to an acceptance of the research hypothesis with a 94-pct confidence.

For the case $\beta = 0.90$ (table 4), sample means of 0.76 and 0.72 are calculated for f_{RC}. The common population standard deviation has a value of 0.031, and the t-statistic a value of 2.37. Application of Student's test shows there is a 97-pct confidence that the population mean of f_{RC} for nonpropagating cases is greater than that for propagating cases.

The mass fraction M_{RC} for the case $\beta = 0.75$ (table 3) has a sample mean of 0.61 for nonpropagating cases and 0.55 for propagating cases. An analysis with Student's test shows that rejection of the null hypotheses (that there is no difference in the mean value of M_{RC}) has a 12-pct chance of being incorrect. This implies that the research hypothesis that the population mean of M_{RC} is greater for nonpropagating cases than for propagating cases can be accepted with an 88-pct confidence.

For the case $\beta = 0.9$ (table 4), the mass fraction M_{RC} has a sample mean of 0.65 for nonpropagating cases and 0.61 for propagating cases. An analysis with Student's t-test shows that rejection of the null hypothesis has a 5-pct probability of being incorrect, which implies a 95-pct confidence that the population mean of M_{RC} is greater for nonpropagating cases than for propagating cases.

The probabilities with which the research hypothesis can be accepted for the quantities f_{RC} and M_{RC} for both cases, $\beta = 0.75$ and $\beta = 0.9$, indicate there is a significant difference between the samples: The samples belong to distinct populations in which the means for f_{RC} and M_{RC} are greater for nonpropagating than for propagating explosions. The demonstrated significant statistical difference between the samples poses the question as to what maximum values of f_{RC} can be expected for a propagating explosion for the cases $\beta = 0.75$ and $\beta = 0.9$. Based upon the data in table 3 for $\beta = 0.75$, which are represented in figure 2, a mass fraction of 0.75 is the maximum value of f_{RC} that is indicated for propagating explosions. The same result is found for the case $\beta = 0.9$ from figure 3. These maximum values are expected independent of the thickness of float coal dust and the percentage of rock dust in the substratum. Thus, the model suggests that a 75-pct airborne rock dust concentration has a high probability of suppressing a propagating coal dust explosion.

The characterization of coal dust explosions as propagating or nonpropagating according to the mass fraction of rock dust either overtaken by the flame front or available at the flame front should be related to the predicted average temperature over the combustion zone. Equations 19 and 21 were used to predict the average temperature over the combustion zone from the measured pressure distribution ahead of and behind the flame front. These average temperatures are shown in table 5 for various flame locations. As expected, the calculated average temperature over the combustion zone is significantly less than the temperatures in excess of 1,500 K expected for complete coal dust combustion. The most probable reason is the incomplete mixing of the hot combustion products with the reactants. The mean predicted average temperature over the combustion zone for the nonpropagating cases when the flame reached the 250-ft station is 660 K, and the mean predicted average temperature over the combustion zone for the propagating cases when the flame reached the

TABLE 5. - Calculated average temperatures over the combustion zone

Test	Explosion propagation[1]	Flame position, ft	Average temperature, K
1	N	100	870
		200	960
		250	440
2	N	200	810
		250	590
3	P	150	1,200
		250	880
		300	790
4	N	150	800
		200	850
		250	750
5	P	100	1,600
		150	930
		250	620
6	P	100	1,270
		250	880
		300	880
7	N	100	690
		200	740
		250	800
8	P	150	700
		300	660
9	N	150	1,050
		250	720
		300	520
10	P	50	870
		150	1,510
		250	850
11	P	150	1,270
		250	930
		400	820

[1]P = propagating; N = nonpropagating.

250-ft station is 823 K. For the available samples, the mean predicted temperature for the nonpropagating case is less than that for the propagating case. Student's t-test was applied to determine with what confidence the mean predicted temperature for the population of nonpropagating cases is always less than the mean predicted temperature for the population of propagating cases. The confidence level was determined to be 96 pct.

CONCLUSION

The mathematical model developed for the lifting and transport of rock and coal dust from well-defined layers on the mine entry floor showed that for two different rock dust concentrations in the substratum and a fixed layer of float coal dust, the calculated mass fraction of rock dust airborne at the 300-ft station was greater for a nonpropagating dust explosion than for a propagating explosion. It was also shown, with a relatively high confidence, that the calculated average mass fraction of rock dust overtaken by the flame front at the 300-ft station was greater for the nonpropagating cases than for the propagating cases. This analysis was made for two assumed constant ratios of the gas velocity to the flame velocity, namely 0.75 and 0.9. The prescribed distribution of coal and rock dust on the entry floor corresponded to a series of tests reported elsewhere (*5*). The computational results shown in figures 3 and 4 indicated that a 75-pct airborne rock dust concentration has a high probability of suppressing a coal dust explosion.

An evaluation of the average temperature over the test combustion zone was developed from the measured gas pressure throughout the entry. The fact that the average temperature was less than the coal combustion temperature indicates that the combustion zone probably consisted of a mixture of regions in which chemical reaction had occurred and regions that were nearly reaction free. As in the analysis of the mass fraction of rock dust, it was shown with a high confidence level that the mean predicted average temperature over the combustion zone for the nonpropagating tests is less than that for the propagating tests.

Further research is required to model the development of the boundary layer ahead of the combustion zone responsible for the entrainment of the dust from the mine floor and its vertical transport into the cross section of the mine entry. This is necessary to determine the influence of mine entry size and geometry on the propagation of a coal dust explosion through a coal-rock dust mixture. Associated with the additional dimensionality, transverse to the direction of propagation, will be an increased computational complexity.

REFERENCES

1. Cybulski, W. (Coal Dust Explosions and Their Suppression.) Transl. by Z. Zienkiewicz. NTIS: TT-73-54001, 1975, 451 pp.

2. Rice, G. S., and H. P. Greenwald. Coal-Dust Explosibility Factors Indicated by Experimental Mine Investigations, 1911 to 1929. BuMines TP 464, 1929, 45 pp.

3. Nagy, J., and D. W. Mitchell. Experimental Coal-Dust and Gas Explosions. BuMines RI 6344, 1963, 27 pp.

4. Richmond, J. K., and I. Liebman. On the Propagation and Control of Coal Mine Explosions. Arch. Thermodyn. Spalania, v. 8, No. 1, 1977, pp. 27-41.

5. Sapko, M. J., E. S. Weiss, and R. W. Watson. Explosibility of Float Coal Dust Distributed Over a Coal-Rock Dust Substratum. Paper in Proceedings of the 22nd International Conference of Safety in Mines Research Institutes. China Coal Ind. Publ. House, Beijing, 1987, pp. 459-468.

6. Lunn, G. A., and A. F. Roberts. Recent Trials With Coal/Dust Methane Hybrid Explosions. Paper in Proceedings of the 22nd International Conference of Safety in Mines Research Institutes. China Coal Ind. Publ. House, Beijing, 1987, pp. 449-457.

7. Green, A. R., J. Piper, and R. W. Upfold. Computer Simulation of Explosions Underground. Paper in Proceedings of the 21st International Conference of Safety in Mines Research Institutes. A. A. Balkema, Boston, MA, 1985, pp. 603-610.

8. Phillips, H. Flame Acceleration in Vapour Cloud Explosions. Ch. in Modelling and Simulation in Engineering, ed. by B. Wahlstrom and K. Leiviska. Elsevier N. Holland, 1986, pp. 243-249.

9. Vassart, A. Numerical Modelling of Coal Dust Explosions in Coal Mines. Paper in Proceedings of the 21st International Conference of Safety in Mines Research Institutes. A. A. Balkema, Boston, MA, 1985, pp. 595-601.

10. Wingfield, B. G. Regression Analysis of Underground Methane Explosions. M.S. Thesis, WV Univ., Morgantown, WV, 1985, 105 pp.

11. Jones, H. Accelerated Flames and Detonation in Gases. Proc. R. Soc. London, A, v. 248, 1958, pp. 333-349.

12. Landau, L. D., and E. M. Lifshitz. Fluid Mechanics. Addison-Wesley Publ., Reading, MA, 1959, 536 pp.

13. Pickles, J. H. A Model for Coal Dust Explosions. Combust. and Flame, v. 44, 1982, pp. 153-168.

14. Levenspiel, O. Chemical Reaction Engineering. Wiley, 1972, 578 pp.

15. Bagnold, R. A. The Physics of Blown Sand and Desert Dunes. Methenen and Co., London, 1941, 265 pp.

16. Chepil, W. S. Dynamics of Wind Erosion: III. The Transport Capacity of the Wind. Soil Sci., v. 60, 1945, pp. 475-480.

17. Zingg, A. W. Wind-Tunnel Studies of the Movement of Sedimentary Material. Paper in Proceedings of Fifth Hydraulics Conference, June 9-11, 1952. Univ. IA, Iowa City, IA, Bull. 34, 1953, pp. 111-135.

18. Travis, J. G. A Model for Predicting the Redistribution of Particulate Contaminants From Soil Surfaces. Los Alamos Sci. Lab., Los Alamos, NM, Informal Rep. LA-6035-MS, Aug. 1975, 63 pp.

19. Dawes, J. G., and A. H. A. Wynn. The Dispersion of Dust by Blast. Saf. Mines Res. Establ. (G. B.), Res. Rep. 46, 1952, 12 pp.

20. Dawes, J. G. Dispersion of Dust Deposits by Blasts of Air, Part I. Saf. Mines Res. Establ. (G. B.), Res. Rep. 36, 1952, 69 pp.

21. _____. Dispersion of Dust Deposits by Blasts of Air, Part II. Saf. Mines Res. Establ. (G. B.), Res. Rep. 49, 1952, 44 pp.

22. Singer, J. M., M. E. Harris, and J. Grumer. Dust Dispersal by Explosion-Induced Airflow. Entrainment by Airblast. BuMines RI 8130, 1976, 50 pp.

23. Hedley, A. B., and M. E. Hedley. Burning Characteristics of Pulverized Coal. J. Inst. Fuel, v. 38, No. 298, 1956, pp. 492-500.

24. Field, M. A., D. W. Gill, B. B. Morgan, and P. G. W. Hawkesley. Combustion of Pulverized Coal. BCURA, Leatherhead, England, 1967, 413 pp.

25. Ott, L. An Introduction to Statistical Methods and Data Analysis. Duxbury Press, Boston, 1984, 775 pp.

APPENDIX A.–NUMERICAL METHOD FOR SOLUTION OF DUST TRANSPORT EQUATION

Equation 9 in the main text is a partial differential equation and, except under very restrictive conditions, precludes an analytical solution. For this reason, a numerical solution must be sought. The mine entry is represented by a linear mesh that is subdivided into increments of constant size Δx, except at the flame front, which requires a variable grid spacing to account for the continuity of the flame motion. The time derivative in equation 9 is represented by a forward time step finite-difference approximation, over a time increment Δt, and the convective term by an upwind spatial difference operator. A central spatial difference is used for the dispersion term. These finite-difference techniques reduce equation 9 to coupled algebraic equations extending from the moving flame front to the exit of the mine entry. At the discrete nodes of the mesh, denoted by the index J, the mass densities ρ_k^n (J) are defined at the nth time step. The finite-difference techniques discussed above reduce equation 9 to the following algebraic equation:

$$\rho_k^{n+1}(J) = \rho_k^n(J) - \frac{\Delta t}{\Delta x}\left(\rho_k^n(J)\,u^n(J) - \rho_k^n(J-1)\,u^n(J-1)\right)$$

$$+ \frac{\Delta t}{(\Delta x)^2} D\rho_4^n(J)\left[\frac{\rho_k^n(J+1)}{\rho_4^n(J+1)} - 2\frac{\rho_k^n(J)}{\rho_4^n(J)} + \frac{\rho_k^n(J-1)}{\rho_4^n(J-1)}\right] + \Delta t\dot{r}_k, \qquad \text{(A-1)}$$

for k = 1,4,

where ρ_k = mass density for species k, $g \cdot cm^{-3}$,

J = integer number of node in mesh,

Δt = time increment, s,

Δx = spatial grid step, cm,

u = gas velocity, $m \cdot s^{-1}$,

D = diffusion coefficient, $cm^2 \cdot s^{-1}$,

and $\dot{r}_k$ = production term for mass species k, $g \cdot cm^{-3} \cdot s^{-1}$.

The boundary conditions are (1) at the moving flame front the mass species is conserved and (2) at the exit a continuity of mass species is assumed. For the cases considered in this study, sonic disturbances generated by the flame front have not reached the exit.

Equation A-1 is explicit in time for the convection and dispersion terms. The source term depends upon the total airborne density at the nth time step, and consequently, the entire equation is explicit in time. The time step was selected to be less than the smallest spatial interval divided by the maximum gas velocity in the entry and was updated throughout the computation to account for the variable grid mesh adjacent to the flame front. The explicit character of the model transport equation excludes any excess computations to develop a solution at the n+1st time step from the density values at the nth time step. The mass species at the flame front is evaluated from a linear interpolation based upon values of the mass species immediately in front of the flame. The mass fraction of coal and rock dust at any location in the entry is determined from the values $\rho_1(x,t)$ and $\rho_2(x,t)$.

APPENDIX B.–NOMENCLATURE

a	parameter in kinematic expression for flame position, $m \cdot s^{-1}$
A	cross-sectional area of mine entry, m^2 or cm^2
b	exponent of time in kinematic expression for flame position, 1
c_o	isentropic sound speed, $m \cdot s^{-1}$
C_p	coal particle specific heat, $cal \cdot g^{-1} \cdot K^{-1}$
d	equivalent diameter, m
D	diffusion coefficient, $cm^2 \cdot s^{-1}$
f	rock dust mass fraction in substratum, 1
f_{RC}	mass fraction of airborne rock dust, 1
h	entry height, cm
h_o	float coal dust layer, mm
h_1	thickness of coal and rock dust substratum layer, mm
h_2	thickness of substratum and float coal dust layer, mm
ℓ	entry length, m or cm
ℓ_o	coal dust layer length, m
ℓ_1	substratum dust layer length, m
$\dot{m}''$	mass injection rate, $g \cdot cm^{-2} \cdot s^{-1}$
m_A	mass of gas ahead of flame front, g
m_B	mass of gas in combustion zone, g
m_o	initial mass of gas in entry, g
M_C	coal dust mass overtaken by combustion zone, g
M_R	rock dust mass overtaken by combustion zone, g

M_{RC}	rock dust mass fraction overtaken by combustion zone, 1
n_k	number of data values in sample k, 1
$P(x,t)$	gas pressure, $dyne \cdot cm^{-2}$
P_o	ambient gas pressure, $dyne \cdot cm^{-2}$
$\dot{r}_k$	production term for mass species k, $g \cdot cm^{-3} \cdot s^{-1}$
R	dust particle radius, cm
R_e	Reynolds number, 1
R_g	gas constant, 8.3143×10^7 $erg \cdot K^{-1} \cdot mol^{-1}$
S	entry floor surface area, cm^2
S_d	estimate of common population standard deviation
S_k^2	kth sample variance, 1
t	time, s
t_α	value of t-statistic for a probability α, 1
t_s	time of shock formation, s
$\overline{T}_B(t)$	average temperature in combustion zone, K
T_o	initial gas temperature, K
$u(x,t)$	gas velocity, $m \cdot s^{-1}$
u^*	wall friction velocity, $m \cdot s^{-1}$
u_f	gas velocity at flame front, $m \cdot s^{-1}$
v_f	flame velocity, $m \cdot s^{-1}$
V	entry volume, cm^3
W	gas molecular weight, 1
x	position coordinate, m
x_f	flame position, m

x_s	shock front location, m
$\bar{y}_k$	kth sample average, 1
α	probability of incorrect rejection of the null hypotheses, 1
β	ratio of gas to flame velocity, 1
γ	adiabatic exponent, 1
Δt	time increment, s
Δx	spatial grid step, cm
λ_c	coal particle thermal conductivity, $cal \cdot cm^{-1} \cdot s^{-1} \cdot K^{-1}$
μ	dynamic viscosity, $g \cdot cm^{-1} \cdot s^{-1}$
ρ_B	bulk density, $g \cdot cm^{-3}$
ρ_C	coal dust particle density, $g \cdot cm^{-3}$
ρ_k	mass density for species k, $g \cdot cm^{-3}$
ρ_R	rock dust particle density, $g \cdot cm^{-3}$
τ_1	time constant for particle heating, s
τ_2	time constant for devolatilization and combustion, s
τ_3	time constant for turbulent mixing, s
ϕ	porosity, 1

* U.S. GOVERNMENT PRINTING OFFICE: 611-012/00,015

INT.-BU.OF MINES,PGH.,PA. 28820